Optical properties and microstructure of gold—fluorocarbon-polymer composite films

J. Perrin,* B. Despax,† and E. Kay
IBM Research Laboratory, 5600 Cottle Road, San Jose, California 95193
(Received 25 January 1985)

The optical transmittance of plasma-deposited composite gold—fluorocarbon-polymer thin films is analyzed in terms of effective-medium theories. The effect of increasing gold volume fraction is shown to be correctly described by the Sheng model, provided the gold-cluster and polymer-inclusion sizes and shapes analyzed by transmission electron microscopy are properly taken into account. Moreover, good consistency is obtained between the present results and our previous study of the electrical conductivity variation at and above the percolation threshold. An extension of the Sheng model has been developed to deal with three-phase systems and has been applied in this work to test the possible existence of an interfacial carbon layer at the gold-polymer interface. The effects of topological disorder and higher-order multipole interactions between the clusters are discussed. Annealing of the films above the glass transition temperature of the polymer results in a drastic change of the film optical properties which is attributed to an increase of gold volume fraction, due to the collapse of the polymer phase, and above all to a modification of the cluster sizes and shapes by sintering and coalescence of gold particles as confirmed by transmission electron microscopy.

I. INTRODUCTION

The optical properties of discontinuous metallic films or granular composite films, consisting of metal clusters embedded in a dielectric, have been of interest since the beginning of the century when Maxwell-Garnett[1] described the first theoretical framework to explain the resonant absorption or dielectric anomaly which characterizes such systems. In this theory (referred to hereafter as MG theory), the dielectric function of the composite medium is related to the polarizability of a single metallic particle surrounded by the dielectric via the Clausius-Mossotti (CM) equation. There have been numerous investigations on Cu, Ag, and Au discontinuous films[2], Au or Ag colloidal particles,[3,4] or cermet films[5] such as Ag-SiO_2 or Au-SiO_2 to verify the applicability of the MG theory. Although this theory correctly predicts the position of the anomalous absorption peak in the visible region at low metal volume fraction and for small spherical particles, it fails to describe the evolution of the optical-absorption spectrum at high metal volume fraction when the metal clusters are interconnected and no longer spherical. This limitation comes essentially from the fact that the MG theory does not treat the metal and the dielectric phase on a symmetrical basis as a function of volume fractional changes. For this reason, no percolation threshold is predicted in the electrical conductivity. In spite of these intrinsic limitations, the MG theory has been refined to take into account the effect of particle shape in the form of ellipsoids,[3,5] the effect of multipole interactions between spherical particles,[6–9] and more recently the effect of topological disorder.[10] The particular case of the two-dimensional island-film structure has also received attention by solving the Clausius-Mossotti problem for a two-dimensional lattice.[11,12] The effect of oxide coatings or adsorbed gases on the metallic particles[13] has also been considered, as well as modified substrate dielectric properties for discontinuous metallic films.[3]

Instead of using the Clausius-Mossotti approach to compute the dielectric constant of a composite medium, Bruggeman[14] initiated the effective-medium-theory (EMT) formalism. The EMT approach, which has been generalized by Stroud,[15] involves two steps:

(i) The definition of microscopic structural units, composed of the known reference materials involved in the composite medium. These structural units must reflect the microstructure of the medium by their shapes. They are supposed to be embedded in a host material which is the so-called effective medium (EM). The expressions of the depolarization electric field induced in the EM by each unit are then derived by solving the Poisson equation with adequate boundary conditions.

(ii) The derivation of the EM dielectric constant from the self-consistency conditions which require that the macroscopically averaged depolarization field for randomly distributed structural units vanish.

In the Bruggeman model, the structural units are spheres, or more generally, ellipsoids of each component and their probability of presence in the EM is simply their respective volume fractions. In the case of a metal-dielectric composite medium, this model does predict a percolation threshold for the electrical conductivity, but does not describe correctly the optical dielectric anomaly predicted by the MG theory. Even with some refinements such as the introduction of effective depolarization factors[16] or retardation effects,[17] the Bruggeman model remains inadequate for the description of optical properties.

A better understanding of the reasons which do make the MG theory successful in predicting the dielectric anomaly has come from the realization that the MG equation can be derived from an EMT model in which one structural unit is made to consist of metal coated with dielectric and embedded in the EM.[18,19] Sheng showed

then, by using a pair-cluster EMT model,[19] that the dielectric anomaly is due to the short-range interaction between nearest-neighbor grains of metal and dielectric. Both the pair cluster and the MG models take into account explicitly the metal-dielectric interface at a microstructural level, whereas the Bruggeman model considers only metal-EM and dielectric-EM interfaces.

Another EMT model has been proposed by Sheng[20] to incorporate the advantages of both the MG and Bruggeman models. Two MG types of structural units consisting, respectively, of metal coated with dielectric and dielectric coated with metal are considered. In each unit, the volumes occupied by each component are proportional to their volume fractions. The probabilities of occurrence of these units have been related to a single growth model of cermet films where diffusion and coalescence of each phase take place.

In this paper, we present a study of the optical properties of cermetlike films consisting of gold clusters embedded in a fluorocarbon polymer. These films are produced by plasma polymerization of a fluorocarbon monomer and simultaneous deposition of gold by sputtering from a gold target. Such a composite material is chemically inert, but its granular microstructure is very sensitive to annealing due to a relaxation of the polymer and the mobility of the polymeric chains above the glass transition temperature, which allows diffusion, sintering, and coalescence of the gold clusters. In a recent study,[21] we have shown that the behavior of the electrical conductivity of percolating gold-flurocarbon films can be related, using the Sheng model, to the actual microstructure of the gold clusters and polymer inclusions. We apply the same model here to interpret the optical properities of as-deposited and annealed films and show the consistency between the microstructural information derived from electrical data and from optical results. In addition, we analyze the respective influences of the gold-cluster and grain size, the effect of higher-order multipole interactions,[6] and the effect of topological disorder[10] at low metal volume fraction. Finally, we test another EMT model which can be considered as a generalization of the Sheng model to three-phase systems in order to decide if a third phase, i.e., a carbon layer, can exist at the gold-polymer interface as some of the surface chemical analysis would suggest.

In Sec. II we describe the film preparation and experimental characterizations. In Sec. III the various theoretical models are presented. The optical measurements are analyzed in the light of these models in Sec. IV. Finally, the results of this study are summarized and discussed in Sec. V.

II. EXPERIMENTAL RESULTS

A. Film preparation

A convenient method for producing metal-containing plasma-polymerized flurocarbon films and, especially, gold-containing films has been described in several previous papers.[21–23] Only the salient features of this method are reviewed here. A plasma is generated in a perfluoropropane— (C_3F_8) argon-gas mixture, at low pressure (20 mTorr), by means of a capacitively coupled coplanar-diode rf (13.56 MHz) discharge system. The electrode to which the rf power is applied consists of a gold sputtering target, whereas the other grounded electrode holds the temperature-controlled substrates. The plasma decomposition of C_3F_8 and subsequent gas-phase chemistry produces unsaturated $(CF_2)_n$ oligomers which polymerize on the walls. Other C_3F_8-decomposition products are mainly fluorine atoms and CF_3^+ ions. F atoms are etchant species, but in C_3F_8 plasmas the $(CF_2)_n$ density is sufficiently high that plasma deposition dominates on all surfaces not submitted to intense high-energy-ion bombardment, in particular, the grounded electrode holding the substrates. The gold rf-powered target, however, is submitted to energetic CF_3^+- and Ar^+-ion bombardment which considerably enhances the F etching of any carbonaceous deposit so that the gold target is kept clean of fluorocarbon polymer. Consequently, gold atoms are sputtered from this target at a rate depending on the ratio of the Ar to the C_3F_8 partial pressure (for details, see Ref. 24). Simultaneous deposition of polymer and gold on the grounded electrode results in the growth of a composite film in which the gold volume fraction p is simply controlled by adjusting the Ar and C_3F_8 flow rates in the reaction chamber. The total growth rate is about 0.5 Å s^{-1} for a rf power of 50 W.

Films of thicknesses ranging from 600 to 1300 Å were deposited at room temperature on fused-silica substrates for optical measurements. Other thin films (150 Å) were deposited on mica foils to allow transmission electron microscopy after removal of the substrate by flotation.

All the below-mentioned characterizations were performed at room temperature both on as-deposited and annealed films. The annealing procedure consisted of a linear temperature ramp up to 180 °C during 1 h followed by 2 h at 180 °C. This annealing temperature was chosen to be slightly above the glass temperature $T_g = 160$ °C of the plasma-polymerized polymer (conventionally designated as plasma-polymerized polytetrafluoroethylene or PPTFE), but below its melting point $T_m = 330$ °C to avoid gold precipitation. The value of T_g has been recently determined by differential scanning calorimetry.[25]

B. Determination of gold volume fraction

The gold volume fraction p in each film was determined by weighing the samples before and after deposition. Knowing the film thickness t measured by the stylus method and the film area, the film density $S(p)$ is computed, and p is derived from the relation

$$p = [S(p) - S_{CF_y}] / [S_{Au} - S_{CF_y}] , \quad (1)$$

where S_{Au} and S_{CF_y} are the bulk gold and PPTFE densities, respectively. The limiting values of $S(p)$, namely, S_{Au} and S_{CF_y}, have been measured independently by the weighing procedure on pure sputtered gold films and pure PPTFE films. The overall precision on p is estimated to be ± 0.03 and the thickness-measurement precision is 20 Å. The thickness measurements were independently confirmed by the optical waveguide method to be described below.

C. Relaxation of the polymer upon annealing

Although no loss of film weight can be detected after annealing, the film thickness t decreases significantly depending on the initial gold volume fraction. Whereas pure-gold films do not contract, pure PPTFE films collapse by about 35% upon annealing. This has been observed by measuring the thickness decrease by the stylus method or from the shift of optical guided modes as explained below. The film collapse must therefore be attributed to a contraction of the polymer phase. A tentative explanation is that PPTFE is produced in a metastable state which relaxes upon annealing. During the cooling process, the polymer returns to an equilibrium state via molecular-chain rearrangement which favors a more compact network. As a confirmation of this hypothesis, we have observed by differential scanning calorimetry[25] that a pronounced relaxation of pure PPTFE occurs during the first heating cycle with a threshold at about 80 °C. Subsequent heating cycles do not exhibit this relaxation, but exhibit only a second-order transition at 160 °C which is attributed to the glass transition temperature T_g.

The practical consequence of the polymer-phase contraction in gold-containing films is a relative increase of the gold volume fraction after annealing. The measured values of t and p before and after annealing for the series of films analyzed here are given in Table I. It can be seen that the relative increase of p is a decreasing function of the as-deposited value of p. It has also been observed that the collapsing effect at a given as-deposited value of p depends on the initial film thickness: the lower the thickness, the greater the collapse for a constant annealing time. Further studies are necessary to understand this latter effect.

D. Surface chemical analysis by x-ray photoelectron spectroscopy

A quantitative surface chemical analysis of the films was achieved by x-ray photoelectron spectroscopy (XPS) in a Hewlett-Packard 5950B ESCA spectrometer (where ESCA denotes electron spectroscopy for chemical analysis). The samples were analyzed after several days of storage in the air. The chemical composition of the film surface ($\sim$30-Å escape depth for the photoelectrons) involves C, F, Au, and O which are, respectively, identified by the C($1s$), F($1s$), Au($4f_{5/2}$) and Au($4f_{7/2}$), and O($1s$) photoelectron-energy lines. Integrated intensities of the lines, normalized to the respective photoionization cross section of each element, are proportional to the atomic concentrations.

A characteristic feature of PPTFE is the five-peak structure of the C($1s$) spectrum which extends from the 284-eV reference energy of bulk carbon up to 294 eV. The four additional peaks have been attributed to the energy shifts induced by the various bonding configurations between carbon and fluorine: C—CF, CF, CF_2, and CF_3 in order of increasing energy shift.[26,27] They reveal the cross-linked structure of PPTFE which contrasts with the single-CF_2 configuration of conventional polytetrafluoroethylene (PTFE). The spectra of C($1s$) obtained on PTFE (Teflon), pure PPTFE, and gold-containing PPTFE are given in Fig. 1. For PTFE, a single CF_2 peak is present and the [F]/[C] ratio (where $[\cdots]$ denotes atomic concentration) and is proportional to integrated intensity) is 2, which indicates that the surface chemical composition is identical to the bulk composition. For pure PPTEFE, the five-peak intensity distribution is identical to that reported in other studies[26,27] and

TABLE I. Measured values of film thickness t and gold volume fraction p for the series of as-deposited and annealed films, the transmittance spectra of which are shown in Figs. 5(a)—5(f). In addition, the values of the parameters used in the computation of the transmittance spectra are given according to the Sheng model. The shape of the polymer-coated gold unit is taken as spherical for both as-deposited and annealed films, $\gamma_m = 1$.

	Experimental		Best-fit parameters			
Sample	t (Å)	p	t (Å)	p	γ_i	x (Å)
			As-deposited			
a	600	1.00	600	1.00		50
b	650	0.91	640	0.90	0.045	40
c	600	0.62	610	0.62	0.045	35
d	610	0.52	620	0.53	0.045	30
e	1100	0.34	1100	0.36	0.045	28
f	1240	0.17	1240	0.16	0.045	25
			Annealed			
a	600	1.00	600	1.00		150
b	620	0.95	620	0.95	0.35	140
c	470	0.79	470	0.79	0.35	120
d	470	0.68	470	0.70	0.35	110
e	780	0.48	780	0.48	0.35	100
f	700	0.29	690	0.31	0.35	70

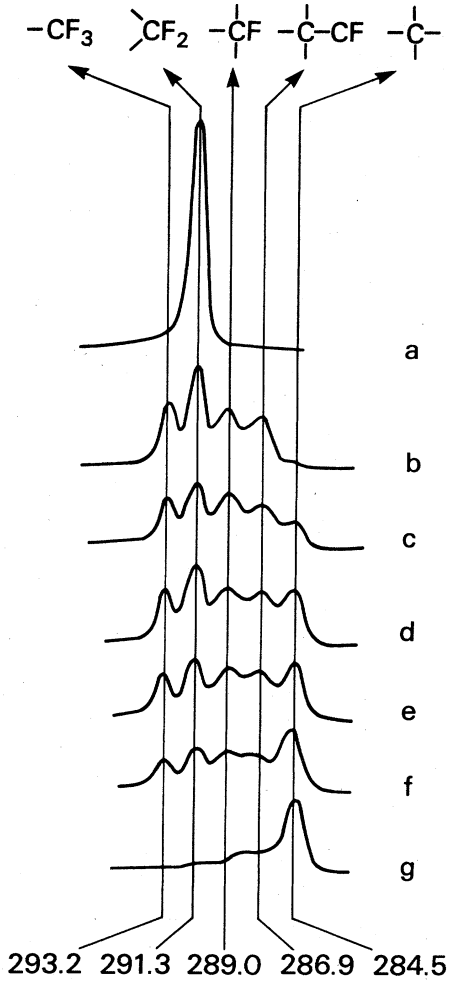

FIG. 1. X-ray photoelectron spectra of C(1s): (a) conventional polytetrafluorethylene (PTFE) (Teflon), (b) plasma-polymerized PTFE, (c) gold-containing polymer $p=0.1$, (d) $p=0.2$, (e) $p=0.4$, (f) $p=0.52$, and (g) $p=0.75$.

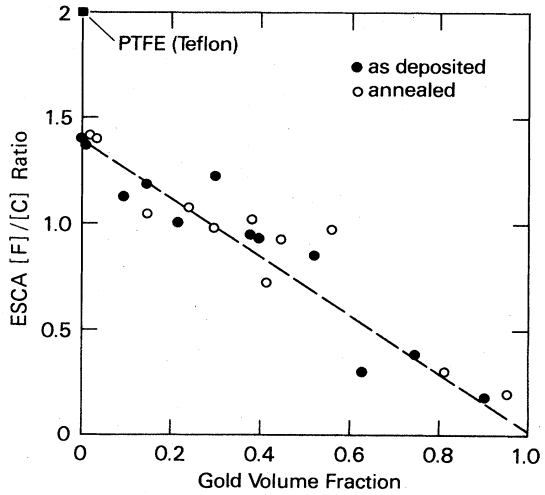

FIG. 2. Ratio of the F(1s) and C(1s) XPS intensities, normalized for their respective photoionization cross sections, as a function of gold volume fraction in the film.

the [F]/[C] ratio is 1.4 ± 0.05. However, the C(1s) spectrum is modified as the gold concentration in the film increases and the first peak at 284 eV becomes more and more important. This is accompanied by a decrease of the [F]/[C] ratio, as shown in Fig. 2. After annealing, the pure PPTFE spectrum remains unchanged, but in gold-containing samples, the 284-eV peak increases. This increase is consistent with the relative increase of the gold volume fraction since the [F]/[C] variation as a function of p is similar for as-deposited and annealed samples (see Fig. 2). The question to be answered is whether this [F]/[C] ratio is indicative only of the surface composition as probed by ESCA or whether it represents a true bulk composition. Unfortunately, it was not possible to make a conclusive depth-composition profiling by sputtering the films with an ion gun in the ESCA apparatus due to the preferential sputtering of fluorine, which destroys the polymer (after sputtering, the C(1s) spectrum of a pure PPTFE film consists essentially of the 284-eV peak, and the [F]/[C] ratio drops). The hypothesis of a bulk effect could be interpreted as the existence of a carbon layer around the gold clusters as if the gold-polymer interface would necessarily involve the transition from a graphitic- or glassy-carbon network before the branching of the cross-linked fluorocarbon. During deposition this would mean either that the $(CF_2)_n$ oligomers would partially decompose in contact with gold clusters or that atomic carbon produced in the plasma would preferentially adsorb on the gold. However, several arguments tend to favor the hypothesis of a surface contamination of the film by a preferential adsorption of carbon on the free surface of gold clusters. Firstly, a pure gold film deposited by sputtering in a pure-argon plasma also exhibits a carbon peak. Secondly, a bulk effect arising from the deposition process would be hardly compatible with the fact that an increase of the carbon peak is observed after annealing. Thirdly, the [Au]/[F] XPS intensity ratio was shown to be proportional to $p/(1-p)$, where p was determined by x-ray fluorescence.[23] As a confirmation of this preliminary evidence, we will show in Sec. IV that the analysis of optical transmittance spectra with an adequate model also allows a ruling out of the bulk hypothesis. The small amount of oxygen (a few percent of the fluorine concentration) is attributed to the oxidation of PPTFE in the air after deposition. Indeed, it has been demonstrated that PPTFE is produced with a large number of molecular and structural defects such as free radicals or dangling bonds which are rapidly passivated in the presence of oxygen via the formation of C=O bonds.[28]

Several XPS studies on small metal clusters evaporated on various substrates have shown binding-energy shifts and line broadenings depending on the substrate-cluster interaction and the cluster size.[29] We have studied the broadening of the Au($4f_{7/2}$) lines as a function of gold volume fraction which is related to the cluster size (see below). The linewidth [full width at half maximum (FWHM)] was found to be fairly constant (~0.92 eV) for

bulk gold or gold-rich films and resulted from the intrinsic lifetime broadening and the spectrometer resolution. However, as p decreased below 0.4 (approximately the percolation threshold[21]), the linewidth increased rapidly up to 1.3 eV for $p=0.15$. Such a broadening is consistent with the observations of Ascarelli *et al.*[30] for small gold clusters evaporated on Teflon. These authors proposed a theoretical explanation in terms of the reduced screening of the final-state core-hole potential as the cluster radius decreases.

E. Transmission electron microscopy (TEM)

TEM on as-deposited and annealed gold-PPTFE films has been thoroughly investigated in our previous study on electrical properties.[21] We present in Fig. 3 a few TEM pictures of low and high gold volume fraction films in order to introduce the analysis of cluster size and shape which will play an important part in the interpretation of optical transmittance spectra.

At low p, the gold clusters appear fairly spherical. As p approaches the percolation threshold p_c, which has been found to be 0.37 ± 0.03 for as-deposited films, and 0.42 ± 0.03 for annealed films,[21] wormlike gold clusters develop, and above p_c a labyrinthlike structure is created where the polymer "wraps" the branches of the gold clusters. In the high-p limit the material can be described as having very flat and elongated polymer inclusions in gold. Annealing induces a dramatic change of the film microstructure in terms of both cluster shape and size. The proposed mechanisms[21] are (i) the motion of gold particles in the polymer above T_g since the rigidity of the matrix is relaxed due to molecular segment mobility, and (ii) the sintering and coalescence of particles entering into contact. At low p, the motion of distant particles before entering into contact is the limiting step since the time for complete coalescence of small touching particles is very small compared to the annealing time. At high p, the gold clusters are already interconnected, which allows further sintering and coalescence. Successive coalescence processes will, however, come to an end since the time required for sintering increases rapidly with the particle size.

A distinction has to be made between gold-cluster size (designated hereafter by its radius r or its semiaxes a,b,c for ellipsoids) and the gold-crystal grain size (designated by a mean diameter x). A cluster-size distribution analysis in a low-p as-deposited film is presented in Fig. 4. From the density distribution [Fig. 4(a)], the volume-fraction distribution [Fig. 4(b)] is derived [by multiplying the numbers in the histogram of Fig. 4(a) by the respective averaged particle volumes] and one deduces the mean

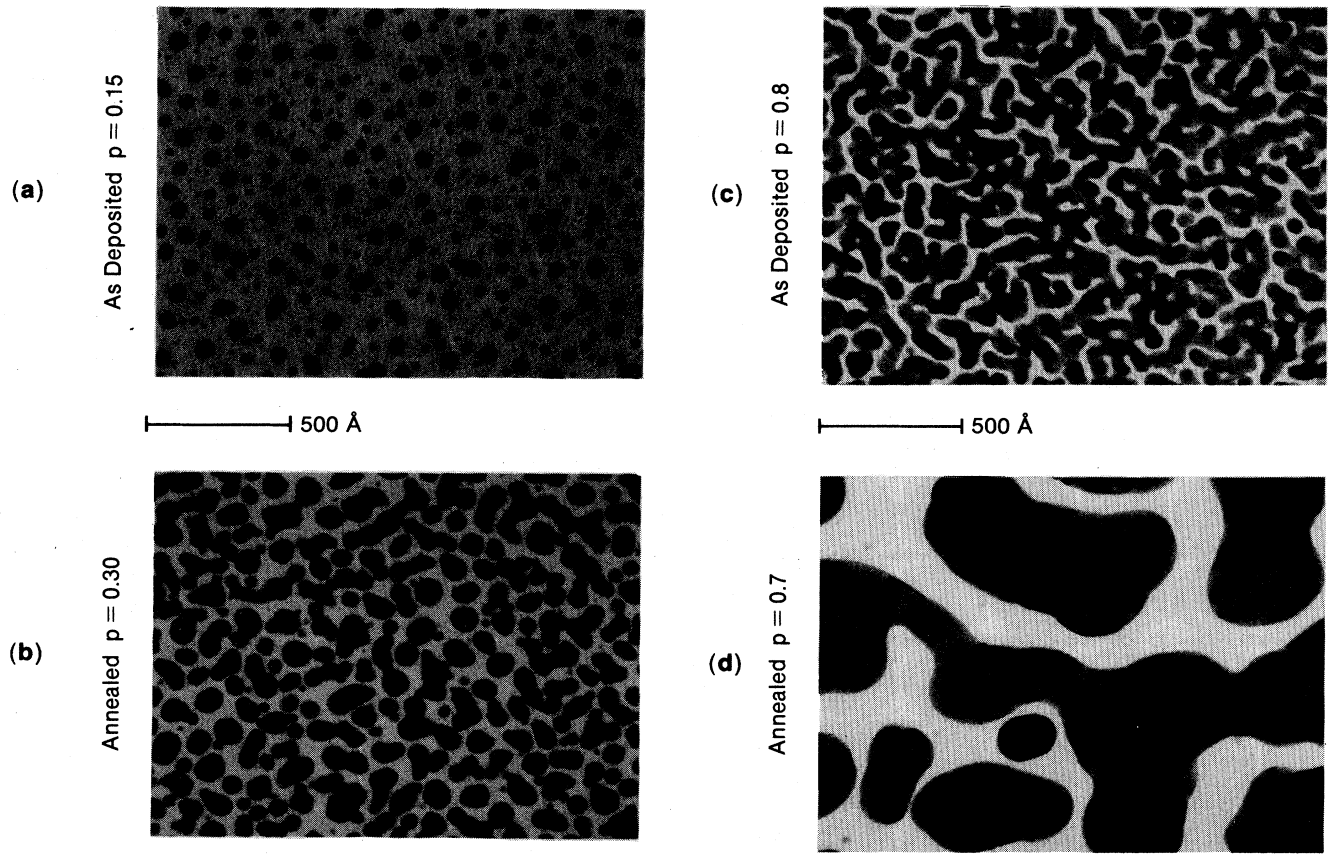

FIG. 3. Transmission electron microscopy (TEM) pictures of as-deposited [(a) and (c)] and annealed [(b) and (d)] films: (a) $p=0.15$, (b) $p=0.3$, (c) $p=0.8$, and (d) $p=0.7$.

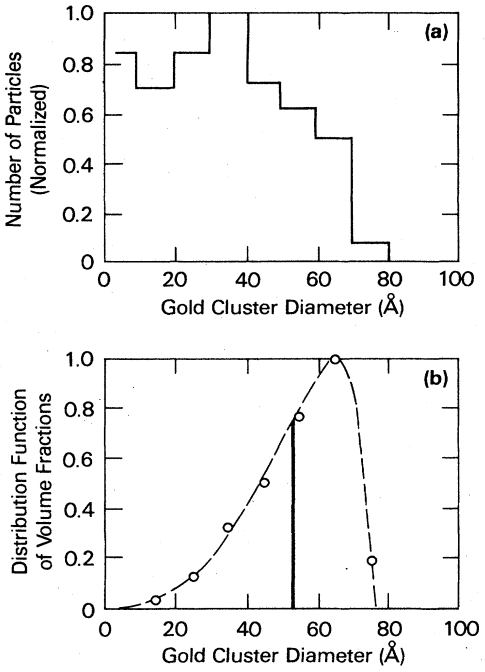

FIG. 4. (a) Distribution of the number of gold particles per unit surface as a function of gold-cluster diameter from the TEM picture of Fig. 3(a). (b) Distribution function of gold volume fraction as a function of gold-cluster size in a polymer-rich film ($p=0.15$). The mean cluster size is given by the position of the thick line.

cluster size, 55 Å. The mean grain size, however, is likely to be smaller since the TEM picture in Fig. 3(a) shows contrast lines through the biggest particles, indicating twinning or other kinds of defects. The same remark applies to the other TEM pictures. A determination of the mean crystallite size for the series of samples presented in Table I will come out of the analysis of the optical transmittance spectra.

F. Optical measurements

The normal-incidence optical transmittance spectra of the six samples presented in Table I were recorded for wavelengths between 300 and 1500 nm, before and after annealing, using a Cary 17 double-beam spectrophotometer. The spectra shown in Figs. 5(a)—5(f) are normalized to the transmittance of a bare fused-silica substrate. At low p [Fig. 5(f)], the spectrum exhibits an absorption peak, the so-called dielectric anomaly characteristic of isolated metallic particles embedded in a dielectric, and no infrared absorption. In high-p [Fig. 5(b)] as-deposited films, this resonance is still present, although shifted to the red, where the infrared (ir) absorption tends to reach the pure-gold behavior. After annealing, two main effects take place:

(i) A strong enhancement of the resonance at low p [Fig. 5(f), dashed curve] characterized by an increased absorption ratio between the maximum and the ultraviolet (uv) region and a reduction of the FWHM of the line. The relative increase of p, due to film contraction on annealing, cannot alone account for these effects, which have to be explained by the microstructural modification of the film as demonstrated in Sec. IV.

(ii) At high p [Fig. 5(b), dashed curve], the resonance

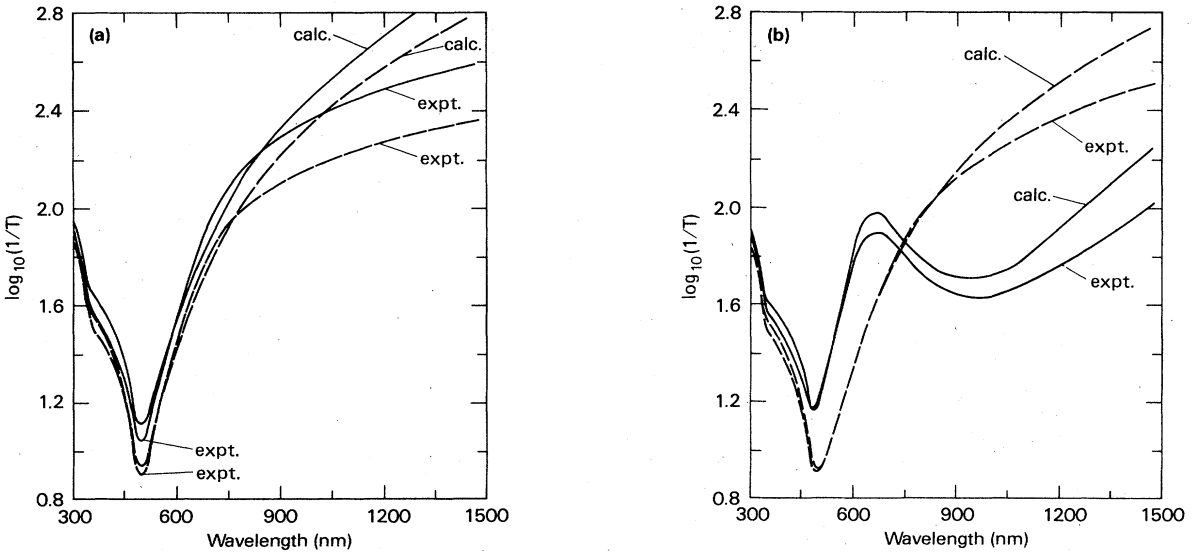

FIG. 5. Experimental and calculated optical transmittance spectra of as-deposited (solid curve) and annealed (dashed curve) films at various gold volume fractions. The experimentally determined volume fractions and film thicknesses, and the parameters used to compute the spectra with the Sheng model are listed in Table I. At low gold volume fraction a comparison is made between the calculated spectra using the Sheng model (S) and the Maxwell-Garnett model (MG).

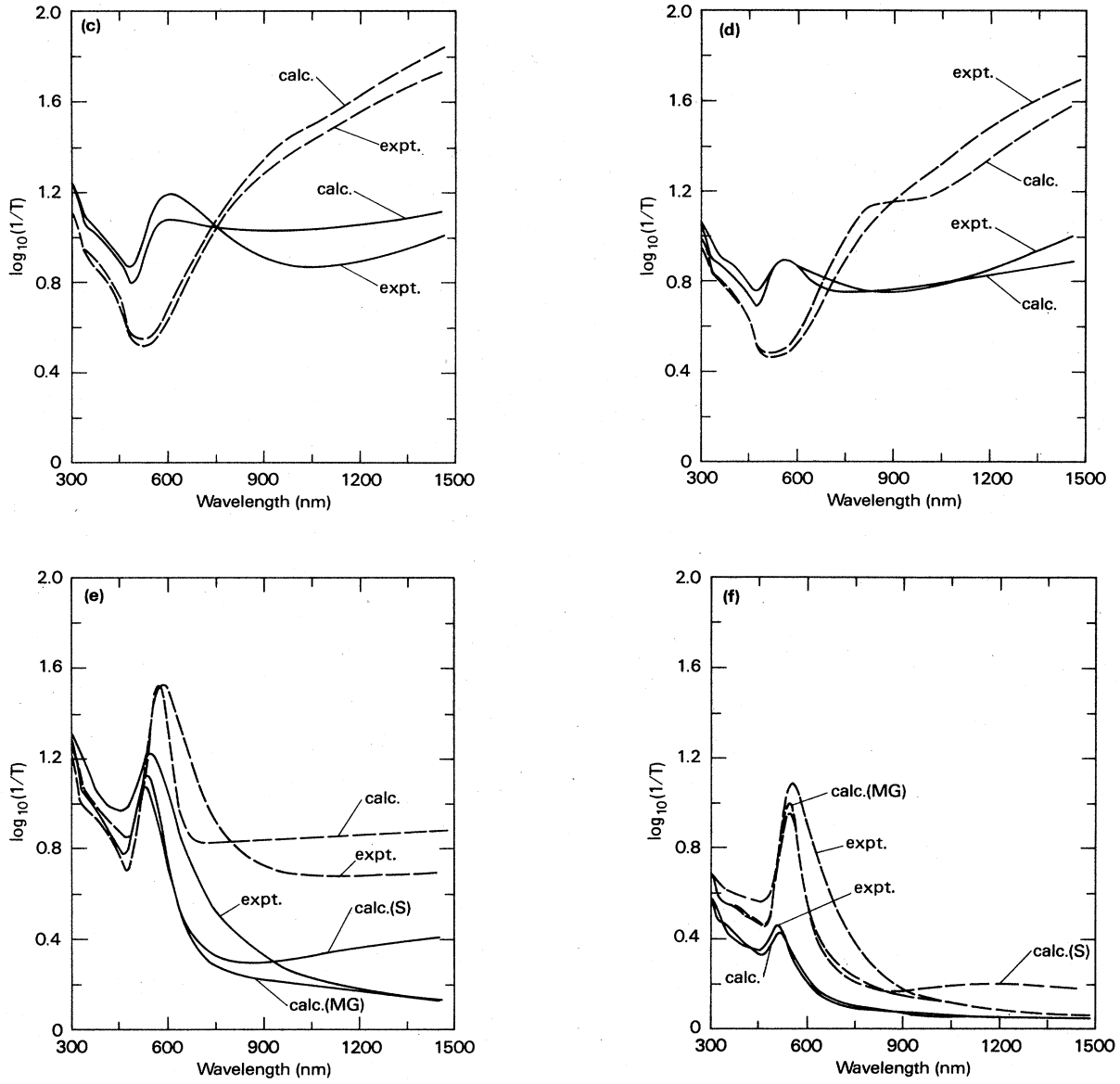

FIG. 5. (*Continued*).

has completely disappeared. The slight but significant decrease of the ir absorption in the pure-gold film [Fig. 5(a)] indicates a grain-size effect.

Figure 6 presents the variations of transmittance, reflectance, and absorbance at 647 nm of a film of intermediate p when submitted to a fast-heating ramp. The drastic inversion between reflectance and absorbance, starting at about 200 °C, reflects the collapse of the polymer phase and the sintering and coalescence of gold clusters. Due to the fast-heating rate, this critical event is delayed to a higher temperature than $T_g = 160$ °C.

TABLE II. Thickness and refractive index of an as-deposited and annealed pure plasma-polymerized polytetrafluorethylene (PPTFE) film, as determined by the optical waveguide method at three laser wavelengths.

PPTFE film	Thickness (Å)	Refractive index $n(\lambda)$ $\lambda=6328$ Å	$\lambda=4880$ Å	$\lambda=4416$ Å
As-deposited	4780	1.367	1.371	1.376
Annealed	3030	1.357	1.368	1.371

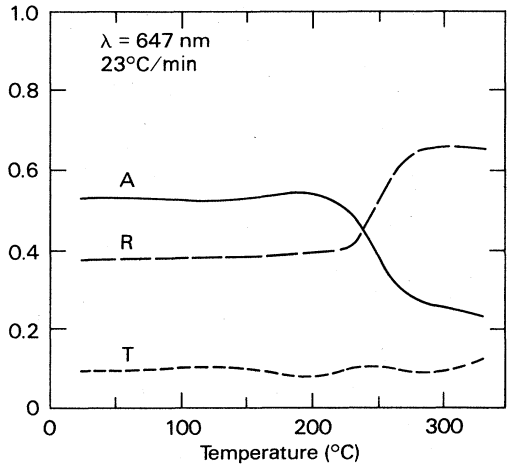

FIG. 6. Variation of transmittance (T), reflectance (R), and absorbance ($A=1-T-R$) of a film as a function of annealing temperature at wavelength $\lambda=647$ nm. The initial gold volume fraction and thickness of the film are $p=0.56$ and $t=650$ Å. The heating rate is 23°C min^{-1}.

Finally, in order to determine the refractive index of PPTFE, we used the optical waveguide method developed to study the optical properties of polymeric thin films.[31] A PPTFE film deposited on a fused-silica substrate was mounted on a prism on a rotating table. A laser beam was transmitted through the waveguide constituted by the film via the coupling prism. The variation of transmitted intensity as a function of the coupling angle for both TE and TM waves presented several resonance peaks characteristic of the guided modes. After analysis at three wavelengths, the thickness and refractive index of the film were unambiguously determined. The results are given in Table II. The thickness decrease after annealing is confirmed and the refractive index shows little variation in the visible region and remains almost unchanged by the annealing process. In the following study, we choose to use a constant value of 1.37 throughout the wavelength range of the optical transmittance spectra. This approximation has a negligible effect on the analysis.

III. THEORY

The applications of the MG theory [from the Clausius-Mossotti (CM) approach] or the EMT are legitimate, provided certain preliminary conditions are fulfilled. The dielectric constants of the reference materials have to be correctly defined, which implies taking into account the effect of finite crystal grain size in the metal and the possible effect of tunneling in the dielectric. The latter effect should be negligible in our case, following the same arguments as Cohen *et al.*[5] used for the case of Ag- or Au-SiO_2 cermet films. The former effect is, however, of considerable importance. Another requirement is that the sizes of the particles or structural units remain smaller than the optical wavelength. Using the EMT approach, Niklasson *et al.*[32] have shown that the MG and Bruggeman models, which retain only the first term in the Mie expansion series of the scattered depolarization field in terms of $(r/\lambda)^{2n+1}$ with $n\geq 1$, are correct to a precision better than 10% if $(r/\lambda)<0.03$. The severity of this restriction is even relaxed at low and high p. Such a condition is largely fulfilled in as-deposited films over the entire range of p. In the case of annealed films, this condition is more critical as shown by the TEM picture in Fig. 3(d). Nevertheless, the first-order approximation will still be made. Another problem is the possibility of many-particle clustering which happens, for example, in colloids[4] but not in our case [see Fig. 3(a)]. We also neglect possible field-retardation effects which have been shown to be of small importance.[17]

A. Effect of grain size on the gold dielectric constant

The dielectric constant of a metal $\epsilon_m(\lambda)$ is decomposed into a free-electron part $\epsilon_m^{(f)}(\lambda)$ and an interband part $\epsilon_m^{(i)}(\lambda)$,

$$\epsilon_m(\lambda)=\epsilon_m^{(f)}(\lambda)+\epsilon_m^{(i)}(\lambda)\ , \tag{2}$$

where

$$\epsilon_m^{(f)}(\lambda)=1-\frac{\lambda^2}{\lambda_0^2}\frac{1}{(1+i\lambda/2\pi c\tau)}\ , \tag{3}$$

according to the Drude theory. Here, λ_0 is the plasma wavelength (133 nm for gold), and τ the mean free-electron relaxation time which is affected by the grain size x. Neglecting quantum-size effects, which are expected to be hardly detectable from optical-absorption measurements,[33] a classical treatment of the electron scattering in a grain gives

$$\tau^{-1}=\tau_b^{-1}+2v_F/x\ , \tag{4}$$

where τ_b is the bulk-metal mean free-electron relaxation time corresponding to a mean free path of 380 Å for bulk gold, and v_F is the Fermi velocity (1.39×10^8 cm s^{-1} for gold). At optical wavelengths, $(\lambda/2\pi c\tau)^2\ll 1$, so that the following approximation can be used:

$$\epsilon_m^{(f)}(\lambda)=1-\frac{\lambda^2}{\lambda_0^2}+i\frac{\lambda^3}{\lambda_0^2}\frac{1}{2\pi c\tau}\ . \tag{5}$$

Assuming that the interband part is not affected by the grain or cluster size, $\epsilon_m(\lambda)$ is simply derived from the bulk dielectric constant $\epsilon_{bm}(\lambda)$ by an addition to the imaginary part

$$\epsilon_m(\lambda)=\epsilon_{bm}(\lambda)+i\frac{\lambda^3}{\lambda_0^2}\frac{v_F}{\pi c x}\ . \tag{6}$$

B. Effective-medium theories

As mentioned in the Introduction, the first step of the EMT approach is to define appropriate structural units incorporating the microstructural information. The MG model corresponds to the structural unit shown in Fig. 7(a). By solving the Poisson equation in ellipsoidal coordinates with boundary conditions at the two interfaces,[34] one obtains the expression of the potential perturbation outside the unit, which is proportional to

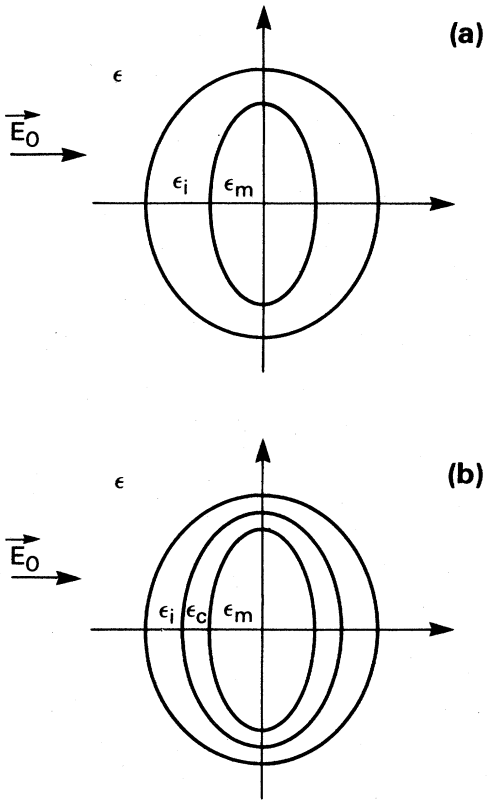

FIG. 7. Cross sections of ellipsoidal and structure units embedded in the effective medium: (a) two-phase confocal unit (gold coated with polymer) used in the Maxwell-Garnett or Sheng model; (b) three-phase confocal unit (gold coated with carbon coated with polymer) used in the modified Sheng model presented here (see text).

$$C=\Phi(L,\epsilon,\epsilon_i,Y^{(1)})=\frac{\epsilon-\epsilon_i Y^{(1)}}{\epsilon(1-L^{(1)})+\epsilon_i Y^{(1)}L^{(1)}}\ , \tag{7}$$

where

$$Y^{(1)}=\Theta(L^{(1)},X^{(1)})=\frac{1+(1-L^{(1)})X^{(1)}}{1-L^{(1)}X^{(1)}}\ , \tag{8}$$

with

$$X^{(1)}=\Psi(p,L^{(0)},\epsilon_m,\epsilon_i)=p\frac{\epsilon_m-\epsilon_i}{L^{(0)}\epsilon_m+(1-L^{(0)})\epsilon_i}\ . \tag{9}$$

The expressions of the depolarization factors $L^{(0)}$ and $L^{(1)}$ are given in the Appendix.

In the Sheng model, the symmetric MG type of unit (insulator coated with metal) with its own ellipsoidal shape is added. The probabilities of occurrence of the units are, respectively, f and $1-f$, where[20]

$$f=\frac{(1-p^{1/3})}{(1-p^{1/3})+[1-(1-p)^{1/3}]}\ . \tag{10}$$

The self-consistency condition for randomly oriented ellipsoids is then

$$f(C_{m,1}+C_{m,2}+C_{m,3})+(1-f)(C_{i,1}+C_{i,2}+C_{i,3})=0\ , \tag{11}$$

where the subscripts m and i refer to the gold unit and insulator unit, respectively, and 1,2,3 stand for the three orientations of the principal axis of the ellipsoids with respect to the applied electric field. For rotational ellipsoids $C_2=C_3$ for both units and Eq. (11) reduces to a fourth-order polynomial equation in ϵ from which the physical solution must be selected.[35]

The three-phase model, which is proposed to treat the problem of a carbon layer at the gold-polymer interface, involves a confocal polymer—carbon-coated-gold unit shown in Fig. 7(b), and a gold—carbon-coated-polymer unit obtained by reversing the internal and external phases. Each unit has its own shape (rotational ellipsoids). The volume fractions are labeled p_m for gold, p_c for carbon, and p_i for polymer. The potential perturbation outside each unit is derived by solving the Poisson equation with boundary conditions as before. For the gold unit, the perturbation is proportional to $C=\Phi(L^{(2)},\epsilon,\epsilon_i,Y^{(2)})$ [Eq. (7)], where $Y^{(2)}=\Theta(L^{(2)},X^{(2)})$ [Eq. (8)], $X^{(2)}=\Psi(p_m+p_c,L^{(1)},\epsilon_c Y^{(1)},\epsilon_i)$ [Eq. (9)], $Y^{(1)}=\Theta(L^{(1)},X^{(1)})$ and

$$X^{(1)}=\Psi(p_m/(p_m+p_c),L^{(0)},\epsilon_m,\epsilon_c)\ .$$

The computation of the three depolarization factors $L^{(0)},L^{(1)},L^{(2)}$ is given in the Appendix. We give the units the same probabilities of occurrence as in the Sheng model and the same self-consistency condition applies.

The three-phase model can be generalized to other systems where all the combinations of confocal layers could be considered, but difficulties arise in the definition of the probabilities of occurrence when more than two units are involved. As far as we know the only previous treatment of coatings on clusters was made for the MG theory in the CM formalism where the polarizability of the coated cluster had to be computed. From a mathematical point of view this corresponds to the computation of the induced field outside a two-phase confocal unit embedded in the dielectric.[13]

IV. ANALYSIS OF OPTICAL TRANSMITTANCE SPECTRA

A. Method of computation of transmittance spectra

In order to simulate the experimental transmittance spectra, a versatile computer program was written. The first step was the computation of the effective dielectric constant ϵ of the film, by selecting one of the models presented above (the Bruggeman model has also been tested but without success) and the entering of the various parameters such as x, p (p_m, p_c, and p_i in the three-phase model), and the shapes of the structural units characterized by the ratio γ of the minor (major) to major (minor) axis for oblate (prolate) rotational ellipsoids. Spherical gold units ($\gamma_m=1$) were always considered because of the TEM observations at low p. The polymer units were treated as randomly oriented oblate ellipsoids ($\gamma_i<1$) since a prolate shape could not account for the electrical conductivity data.[21] For the bulk-gold dielectric constant $\epsilon_{bm}(\lambda)$, we used the tabulated data of Weaver *et al.*[36] In the three-phase model, the carbon layer was considered as

graphitic using the data of Arakawa *et al.*[37] for $\epsilon_c(\lambda)$ (with glassy carbon the results differ slightly but do not contradict the conclusion that the existence of a carbon layer can be ruled out).

The next step was the computation of the transmittance of a film of thickness t on a fused-silica substrate of refractive index computed from the Malitson[38] dispersion formula. The transmittance through the film was computed from rigorous wave-amplitude reflection and transmission equations,[39] but the interferences between the substrate boundaries were relaxed.

B. Application of the Sheng and MG models

As-deposited films are analyzed first. In order to determine the shape parameter γ_i of the polymer unit, the high-p films where the probability $1-f$ is close to 1 [see Eq. (16)] are considered. Figure 8 shows the influence of a variation of γ_i on the transmittance of a film with p and t corresponding to the experimental values measured for sample b and a crystallite size $x=60$ Å, which is the maximum expected value, deduced from the TEM picture in Fig. 3(c). The position of the minimum after the resonance is very sensitive to γ_i and the best agreement with the experimental spectrum in Fig. 5(b) is obtained with $\gamma_i=0.045\pm0.005$. This value is slightly higher than the value determined[21] from electrical data $\gamma_i=0.02$, but in good qualitative agreement as both exclude spherical or prolate shapes. To be consistent with the Sheng model, this value will be kept constant throughout the entire subsequent analysis of as-deposited-film transmittance spectra. The influence of the grain size x under the same conditions is now shown in Fig. 9. The p and t values have been only slightly adjusted within the experimental precision. By comparing the ratio of the resonance maximum to the dip minimum at about 520 nm, the best agreement with the experimental spectrum is obtained with $x=50$ Å. The values of x at lower p are then expected to be smaller or equal to 50 Å. Going now to the lowest-p film (sample f), the influence of x is shown in Fig. 10. The best agreement with the experimental spectrum of Fig. 5(f) is obtained with $x=25$ Å, a value which is one-half the mean cluster size [see Fig. (9b)] and reflects the presence of defects observed on the TEM picture. From the low- and high-p limiting values of x, a linear interpolation gives the grain size at intermediate p

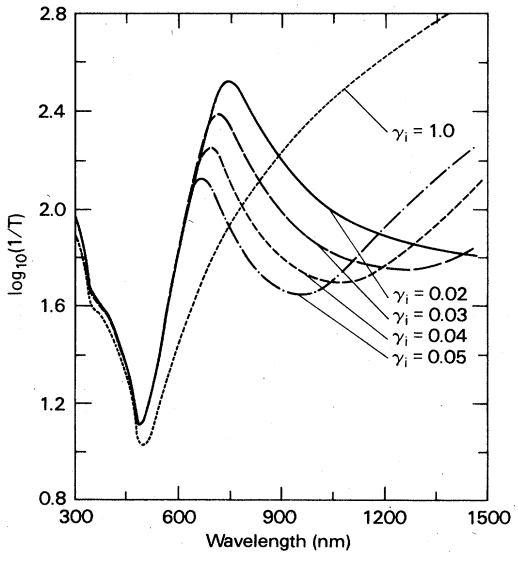

FIG. 8. Influence of the shape of polymer inclusions on the calculated (Sheng model) optical transmission spectrum of a gold-rich film ($p=0.91$) of thickness $t=650$ Å and gold grain size $x=60$ Å. γ_i is the ratio of the minor to major axis of oblate spheroids of polymer coated with gold.

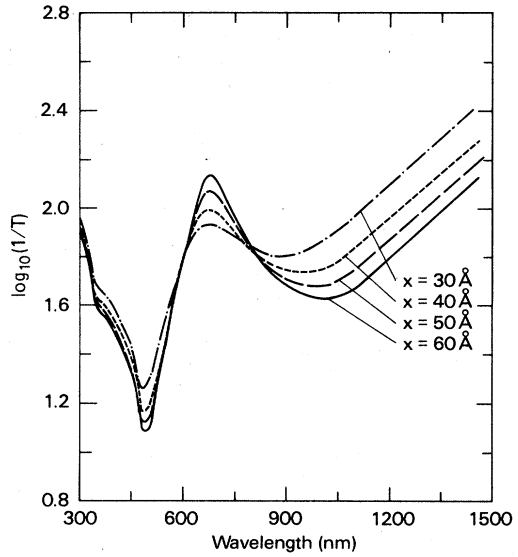

FIG. 9. Influence of the gold grain size on the calculated (Sheng model) optical transmittance spectrum of a gold-rich film ($p=0.91$) of thickness $t=630$ Å using a polymer-inclusion shape characterized by $\gamma_i=0.045$.

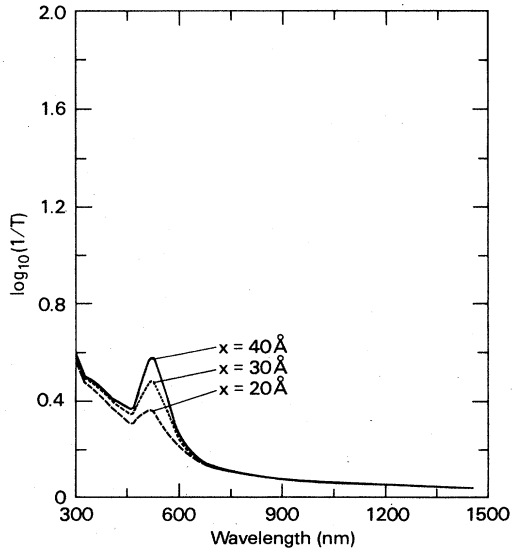

FIG. 10. Influence of the gold grain size on the calculated (Sheng model) optical transmittance spectrum of a polymer-rich film ($p=0.16$) of thickness $t=1240$ Å for spherical gold clusters and oblate polymer inclusions ($\gamma_i=0.045$).

and a grain size of 60 Å is assumed for the pure-gold film (sample *a*). With these parameters and a slight adjustment of p and t (see Table I), all the spectra have been simulated in Figs. 5(a)—5(f). The agreement with experimental spectra is in general very satisfactory. Three types of discrepancies have to be pointed out, however:

(i) The shape of the ir-absorption tail for the pure-gold sample *a* suggests either that the bulk data are not entirely reliable or that the model for electron scattering in the grains is oversimplified. Other effects, such as the presence of voids or surface roughness,[40] or an anomalous skin effect,[41] cannot reconcile the experimental and theoretical curves.

(ii) The Sheng model at $p \sim 0.3$ (sample *e*) tends to give too much emphasis to the gold-coated polymer units which contribute to the ir absorption. This relates to the choice of the probability law given to the units. For comparison, the MG computation at the same volume fraction is also given in Fig. 5(e).

(iii) The experimental resonance peak for sample *e* is much more broadened than the calculated one and no parameter adjustment can reduce the discrepancy. It will be shown below that a topological disorder can partially explain the broadening.

A similar adjustment method has been used to simulate the experimental spectra of annealed films. At first, the lowest-p film was studied to derive the new grain size. The best agreement was obtained with $x = 70$ Å as shown in Fig. 5(f) (dashed curves). Such a size increase is consistent with TEM observations if one refers to Fig. 3(b), which corresponds approximately to the annealed sample *f*. In view of the TEM picture of a high-p annealed film shown in Fig. 3(d), the grain size appears to increase steadily as a function of p. For sample *e*, a value of 100 Å is necessary to account for the height of the resonance peak [Fig. 5(e), dashed curve]. Assuming a regular increase of x up to 150 Å for the pure-gold sample *a*, the only parameter which we have to adjust is the new oblateness of the polymer unit. The value of $\gamma_i = 0.35 \pm 0.05$ was adjusted to fit the very sensitive shape of the absorption dip in the spectra of samples *b* to *d*. The final simulated spectra, using the parameters of Table I, are given in Fig. 5(a)—5(f) (dashed curves). Once again the agreement with experiment is very satisfactory, with still the same remarks concerning the ir-absorption tail of the pure-gold film and the emphasis given by the Sheng model on the gold-coated-polymer unit around $p = 0.3$. The increase of γ_i after annealing is consistent with the results of the electrical data analysis.[21] The value obtained here is nevertheless 4 times larger. As a matter of fact, the analysis of the electrical conductivity variation above the percolation threshold does not take into account any grain-size effect. The model of Mayadas and Shatzkes[42] treats the problem of grain conductivity but it applies essentially to homogeneous polycrystalline films. One can expect, however, that a decrease of grain size as p diminishes can actually result in additional obstacles for the dc current. In the Sheng model, this means an increase of oblateness of insulating units. The fitting value of $\gamma_i = 0.08$ may, therefore, be two low as a description of the actual shape of polymer inclusions since it could account also for the grain-size effect.

Finally, the Sheng model has been tested on the interpretation of the transmittance (T), reflectance (R), and absorbance ($A = 1 - T - R$) measurements at 647 nm during the annealing of an intermediate-p film (see Fig. 6). The computed values for T, R, and A before annealing, using the experimentally measured values $p = 0.56$ and $t = 650$ Å, and taking $\gamma_i = 0.045$ and $x = 30$ Å, are respectively, 0,11, 0.36, and 0.53, which compare very well with the measured values 0.092, 0.38, and 0.53. After the annealing process, the film being destroyed, no measurements of p or t were available. Nevertheless, an excellent agreement with experimental data, $T = 0.12$, $R = 0.65$, and $A = 0.22$, was obtained using the parameters $p = 0.72$, $t = 510$ Å, $x = 110$ Å, and $\gamma_i = 0.35$, which result in $T = 0.16$, $R = 0.65$, and $A = 0.19$.

C. Influence of multipole interactions and topological disorder

The various models[6–9] treating effect of multipole interactions between spherical particles on cubic lattices are all basically derived from a Clausius-Mossotti approach. We retain here the formula given by Doyle[6] for the simple-cubic lattice.

On the other hand, the effect of topological disorder in the lattice, elegantly treated by Liebsch and Persson,[10] can be viewed as replacing a randomly occupied cubic lattice with single-particle polarizability α by a fully occupied lattice with a new effective polarizability which incorporates the disorder via the density of states of the lattice. We consider here the case of a fcc lattice for which the density of states has been tabulated by the authors and allow a maximum disorder by taking a lattice parameter equal to $2^{3/2}r$.

The CM models for multipole interactions and topological disorder are both compared to the standard MG model in the case of the annealed sample *f*. The theoretical curves are shown on Fig. 11. The multipole contribution has little effect on the shape of the resonance peak and is expected, in fact, to be important[6] only above $p = 0.4$. On the contrary, the topological disorder induces a considerable resonance broadening of the same magnitude as in the experimental spectrum shown in Fig. 5(f). However, the red shift of the resonance is too large compared to the very small shift of the experimental spectrum with respect to the MG- or Sheng-computed curves. Liebsch and Persson[10] have shown, however, that their model reproduces almost perfectly the shift and broadening observed by Kreibig *et al.*[4] on Ag colloids at $p = 0.21$. Nevertheless, as the authors noted, the Kreibig results might have been affected by particle clustering and by a suspected wavelength-scale shift. In spite of this ambiguity about the validity of the peak shift predicted by this theory, the broadening effect strongly supports the assumption that the topological disorder plays an important part in experimental systems. There is still a need for a synthetic theory with could incorporate the disorder at low p and the matrix inversion accountered for by the Sheng model.

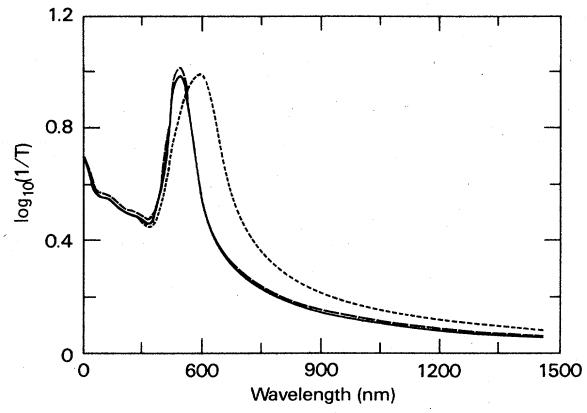

FIG. 11. Calculated optical transmittance spectra for a film of gold volume fraction $p=0.31$, thickness $t=690$ Å, and gold grain size $x=70$ Å using the classical MG model for spherical particles (solid curve), introducing the effect of higher-order multipole interactions (dashed curve) and considering the effect of topological disorder on a fcc lattice (dotted curve).

D. Test of the three-phase model

The three-phase model has been applied to high-p as-deposited films (samples b and c). The experimental values of p determined by weighing do not need to be corrected since the densities of PPTFE (2.3 g cm^{-3}) and carbon (1.8 to 2.3 g cm^{-3} for amorphous or graphitic carbon) are almost identical to and much lower than that of gold. The carbon volume fraction to be introduced in the computation was calculated from the [F]/[C] XPS intensity ratio y estimated from Fig. 2 via the relation

$$y=1.4\frac{p_m}{p_m+p_c}\ . \tag{12}$$

For samples b and c, one obtains $p_c=0.08$ and $p_c=0.21$, which correspond to polymer-to-carbon ratios of 0.25 and 0.8, respectively. The grain sizes are those of Table I. The spectra have been computed for three different values of γ_i: 0.045, 0.01, and 0.001. The results are shown in Fig. 12. No agreement with experimental spectra can be obtained, which confirms that the presence of the peak at 284 eV in C(1s) XPS spectra must be attributed to the contamination of the free surfaces of gold clusters.

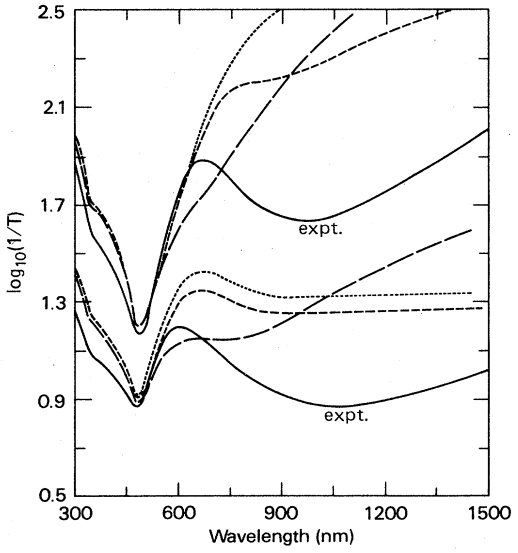

FIG. 12. Comparison between experimental optical transmittance spectra (solid curves) of as-deposited samples b and c (see Table I) and calculated spectra using the modified Sheng model to account for a carbon layer at the gold-polymer interface. Three polymer unit shapes are considered: $\gamma_i=0.045$ (long-dashed curve), $\gamma_i=0.01$ (short-dashed curve), and $\gamma_i=0.001$ (dotted curve). The upper curves correspond to $p=0.9$, $t=640$ Å, and a polymer-to-carbon ratio of 0.25. The lower curves correspond to $p=0.62$, $t=610$ Å, and a polymer-to-carbon ratio of 0.8.

V. SUMMARY AND CONCLUSION

We have shown that a thorough characterization of the physical properties of a composite material, such as gold-PPTFE, combining volume-fraction measurement, microstructural analysis by TEM, and optical transmittance and electrical conductivity measurements, allowed us to test conveniently the applicability of relevant theories. The material system used is particularly interesting because of the strong microstructural modifications that can be induced by annealing. The influence of gold-crystal grain size and polymer-inclusion shape have been shown to determine to a large extent the optical properties. It is absolutely necessary to treat these parameters appropriately in any effective-medium theory. The best agreement with experimental transmittance spectra is obtained with the Sheng model, although the definition of the probability law for the two structural units involved could be improved. The resonance-peak broadening at low gold volume fraction is, however, not accounted for by either the Sheng or the Maxwell-Garnett model. Consideration of topological disorder explains the broadening but induces a red shift of the resonance peak which is not observed experimentally. Finally, we have constructed a three-phase model to study the possible existence of a carbon layer at the gold-PPTFE interface and shown that this hypothesis, suggested by XPS surface chemical analysis, can be ruled out as a bulk effect.

ACKNOWLEDGMENTS

Two of us (J. P. and B. D.) are grateful to the IBM Corporation for financial support. The optical waveguide measurements were made by Mark Jurich, to whom we wish to express our appreciation. Thanks are also due to Virginia Hanchett for the TEM pictures and Art Poenisch for technical assistance.

APPENDIX: COMPUTATION OF DEPOLARIZATION FACTORS

In a three-phase ellipsoidal unit, the depolarization factors $L_1^{(0)}$, $L_1^{(1)}$, and $L_1^{(2)}$ for an electric field parallel to the a axis of the ellipsoid are obtained from the general relation

$$L(\xi)=\frac{R(\xi)}{2}\int_{\xi}^{\infty}\frac{ds}{(s+a^2)R(s)}\ ,$$

where

$$R(s)=[(s+a^2)(s+b^2)(s+c^2)]^{1/2}\ ,$$

ξ being the ellipsoidal coordinate defining the family of surfaces confocal to the ellipsoid of semiaxes a,b,c for which $\xi=0$. The superscripts (0),(1),(2) correspond to the three boundaries in a three-phase unit. The corresponding values of ξ (ξ_0,ξ_1,ξ_2) are related to the volume fractions p_0,p_1,p_2 (from the inside to the outside phase) such as $p_0+p_1+p_2=1$, via the relations

$$\xi_0=0,\quad \frac{p_0}{(p_0+p_1)}=\frac{R(\xi_0)}{R(\xi_1)},\quad \frac{(p_0+p_1)}{(p_0+p_1+p_2)}=\frac{R(\xi_1)}{R(\xi_2)}\ .$$

For rotational ellipsoids ($b=c$), the shape of the unit can be described by the axis ratios $\gamma=\gamma_0=a/b$,

$$\gamma_1=[(\xi_1+a^2)/(\xi_1+b^2)]^{1/2}\ ,$$

and

$$\gamma_2=[(\xi_2+a^2)/(\xi_2+b^2)]^{1/2}\ .$$

For oblate rotational ellipsoids (disklike, $\gamma<1$), the three depolarization factors take the analytical form

$$L_1^{(k)}=[\gamma/(1-\gamma^2)^{3/2}][e_o^{(k)}-\tan^{-1}(e_o^{(k)})]\ ,$$

where

$$e_o^{(k)}=[(1/\gamma_k)^2-1]^{1/2}\ .$$

For prolate rotational ellipsoids (needlelike, $\gamma>1$),

$$L_1^{(k)}=[-\gamma/(\gamma^2-1)^{3/2}][e_p^{(k)}-\tanh^{-1}(e_p^{(k)})]\ ,$$

where

$$e_p^{(k)}=(1-(1/\gamma_k)^2)^{1/2}$$

and

$$\tanh^{-1}(x)=\tfrac{1}{2}\ln\left[\frac{1+x}{1-x}\right]\ .$$

The other depolarization factors for an electric field parallel to the b or c axis are then obtained from the relation

$$L_2^{(k)}=L_3^{(k)}=(1-L_1^{(k)})/2\ .$$

*Permanent address: Equipe Synthese de Couches Minces pour l'Energetique, Ecole Polytechnique, 91128 Palaiseau Cedex, France.

†Permanent address: Laboratoire de Genie Electrique, Universite Paul Sabatier, 118 route de Narbonne, 31067 Toulouse Cedex, France.

[1]J. C. Maxwell-Garnett, Philos. Trans. R. Soc. London **203**, 385 (1904); **205**, 237 (1906).

[2]S. Norrmann, T. Andersson, C. G. Granqvist, and O. Hunderi, Phys. Rev. B **18**, 674 (1978), and references therein.

[3]R. H. Doremus, J. Chem. Phys. **42**, 414 (1965).

[4]U. Kreibig, A. Althoff, and H. Pressmann, Surf. Sci. **106**, 308 (1981).

[5]R. W. Cohen, G. D. Cody, M. D. Coutts, and B. Abeles, Phys. Rev. B **8**, 3689 (1973).

[6]W. T. Doyle, J. Appl. Phys. **49**, 795 (1978).

[7]R. C. McPhedran and D. R. McKenzie, Proc. R. Soc. London, Ser. A **359**, 45 (1978).

[8]A. S. Sangani and A. Acrivos, Proc. R. Soc. London, Ser. A **386**, 263 (1983).

[9]W. Lamb, D. M. Wood, and N. W. Ashcroft, Phys. Rev. B **21**, 2248 (1980).

[10]A. Liebsch and B. N. J. Persson, J. Phys. C **16**, 5375 (1983).

[11]M. J. Dignam and M. Moskovitz, J. Chem. Soc. Faraday Trans. 2 **69**, 56 (1973).

[12]D. Bedaux and J. Vlieger, Physica (Utrecht) **67**, 55 (1973); **73**, 287 (1974).

[13]A. Donnadieu, Thin Solid Films **6**, 249 (1970).

[14]A. G. Bruggeman, Ann. Phys. (Leipzig) **24**, 636 (1935); **24**, 665 (1935).

[15]D. Stroud, Phys. Rev. B **12**, 3368 (1975).

[16]C. G. Granqvist and O. Hunderi, Phys. Rev. B **18**, 2897 (1978).

[17]C. G. Granqvist and O. Hunderi, Phys. Rev. B **16**, 1353 (1977).

[18]G. B. Smith, J. Phys. D **10**, L39 (1977); Appl. Phys. Lett. **35**, 668 (1979).

[19]P. Sheng, Phys. Rev. B **22**, 6364 (1980).

[20]P. Sheng, Phys. Rev. Lett. **45**, 60 (1980); Opt. Laser Technol. **13**, 253 (1981).

[21]J. Perrin, V. Hanchett, and E. Kay, J. Vac. Sci. Technol. A (to be published).

[22]E. Kay and A. Dilks, J. Vac. Sci. Technol. **16**, 428 (1979).

[23]E. Kay and M. Hecq, J. Appl. Phys. **55**, 370 (1984); J. Vac. Sci. Technol. A **2**, 401 (1984).

[24]E. Kay, J. Coburn, and A. Dilks, in *Topics in Current Chemistry* (Springer, Berlin, 1980), Vol. 94, p. 1.

[25]J. Perrin, R. L. Siemens, and E. Kay (unpublished).

[26]D. W. Rice and D. F. O'Kane, J. Electrochem. Soc. **123**, 1308 (1976).

[27]D. T. Clark, A. Dilks, and D. Shuttleworth, in *Polymer Surfaces,* edited by D. T. Clark and W. J. Feast (Wiley, London, 1979).

[28]U. Hetzler and E. Kay, J. Appl. Phys. **49**, 5617 (1978).

[29]M. G. Mason, Phys. Rev. B **27**, 748 (1983), and references therein.

[30]P. Ascarelli, M. Cini, G. Missoni, and N. Nistico, J. Phys. (Paris) Colloq. **2**, 125 (1977).

[31]J. D. Swalen, R. Santo, M. Tacke, and J. Fisher, IBM J. Res. Dev. **21**, 168 (1977); J. D. Swalen, J. Phys. Chem. **83**, 1438 (1979).

[32]G. A. Niklasson, C. G. Granqvist, and O. Hunderi, Appl. Opt. **20**, 26 (1981).

[33]L. Genzel and U. Kreibig, Z. Phys. B **37**, 93 (1980), and references therein.

[34]J. A. Stratton, *Electromagnetic Theory* (McGraw-Hill, New York, 1941), pp. 207–214.

[35]This formulation of the Sheng model differs from that given by the author, but is more convenient for introducing the three-phase model.

[36]J. H. Weaver, C. Krafka, D. W. Lynch, and E. E. Koch, *Optical Properties of Metal—Part II, Physics Data* (Fachinforma-

tionszentrum Energie, Physik, Mathematik Gmbh, Karlsruhe, Germany, 1981), No. 18-2, pp. 59—60.
[37]E. T. Arakawa, M. W. Williams, and T. Inagaki, J. Appl. Phys. **48**, 3176 (1977).
[38]I. H. Malitson, J. Opt. Soc. Am. **55**, 1205 (1965).
[39]See, for example, F. Abeles, in *Advanced Optical Techniques,* edited by A. C. S. Van Heel (North-Holland, Amsterdam, 1967), Chap. V. p. 144.
[40]D. E. Aspnes, E. Kinsbron, and D. D. Bacon, Phys. Rev. B **21**, 3290 (1980).
[41]M. L. Theye, Phys. Rev. B **2**, 3060 (1970).
[42]A. F. Mayadas and M. Shatzkes, Phys. Rev. B **1**, 1382 (1970).

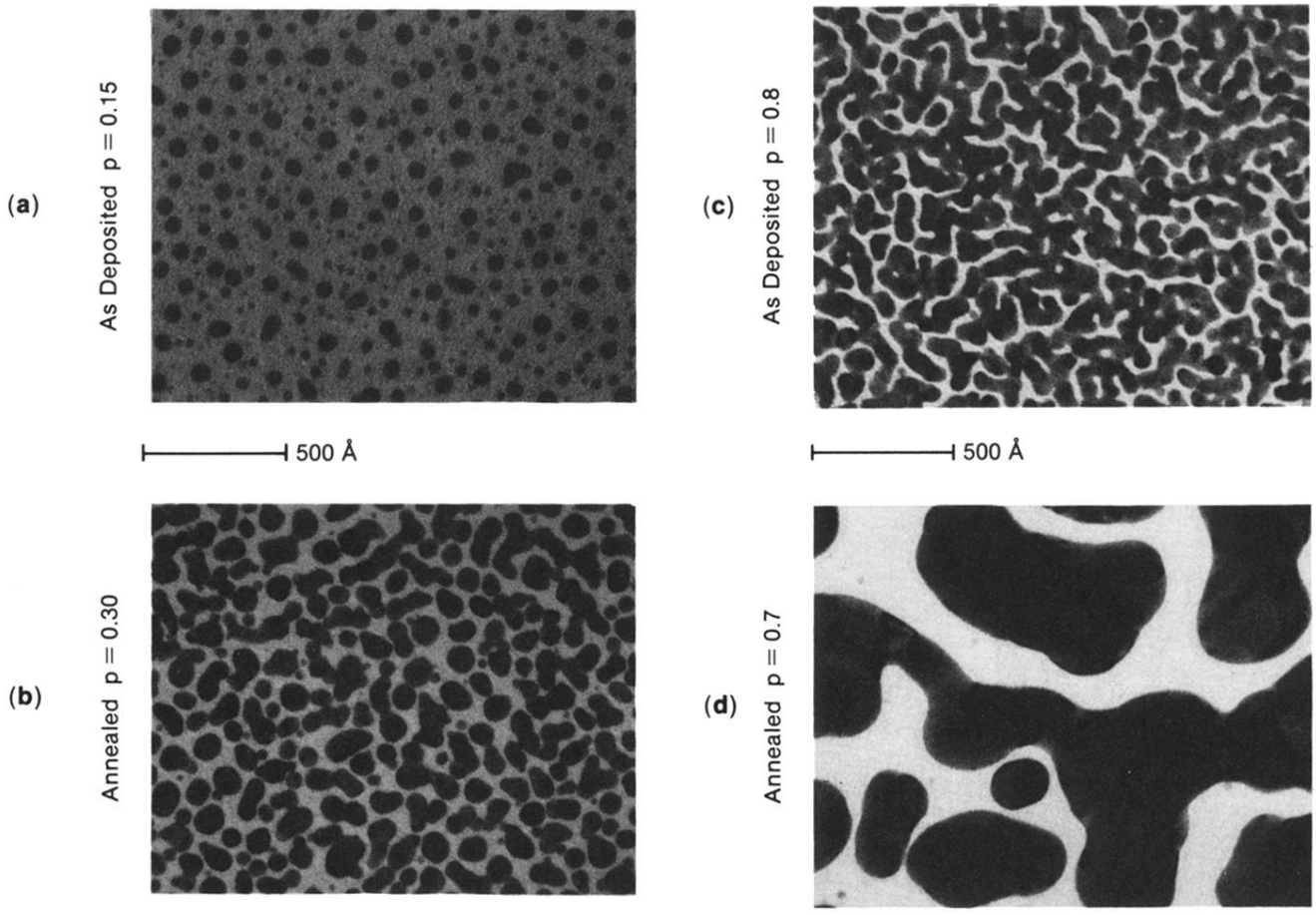

FIG. 3. Transmission electron microscopy (TEM) pictures of as-deposited [(a) and (c)] and annealed [(b) and (d)] films: (a) $p=0.15$, (b) $p=0.3$, (c) $p=0.8$, and (d) $p=0.7$.